Mechanical Engineering Advances 2026, 4(3), 4473.
https://doi.org/10.59400/mea4473

Article

A Unified Analytical Framework for Modal Analysis of Beams with Elastic Supports and End Masses

Ahmed M. Zakwan*, Ibrahim M. Ashqar, Mohamad S. Qatu

GameAbove College of Engineering and Technology, Eastern Michigan University, Ypsilanti, MI 48197, USA
*** Corresponding author:** Ahmed M. Zakwan, azakwan@emich.edu

CITATION

Zakwan, A. M., Ashqar, I. M., Qatu, M. S. A Unified Analytical Framework for Modal Analysis of Beams with Elastic Supports and End Masses. Mechanical Engineering Advances. 2026; 4(3): 4473.
https://doi.org/10.59400/mea4473

ARTICLE INFO

Received: 2 June 2026
Revised: 29 June 2026
Accepted: 17 July 2026
Available online: 28 October 2026

COPYRIGHT

Copyright © 2026 by author(s). *Mechanical Engineering Advances* is published by Academic Publishing Pte Ltd. This work is licensed under the Creative Commons Attribution (CC BY) license.
https://creativecommons.org/licenses/by/4.0/

Abstract: Predicting vibration in beamlike structures with non-ideal supports remain a significant engineering challenge. Classical beam models usually assume perfectly rigid boundaries. Real structures, however, contain flexible supports and attached end components that modify the dynamic response. This study develops a unified analytical framework for the free vibration analysis of Euler–Bernoulli beams with elastic restraints and lumped end masses. The formulation incorporates translational stiffness, rotational stiffness, and rotary inertia within a compact and physically transparent model. Frequency-dependent boundary conditions are assembled into a concise 4 × 4 characteristic matrix. Classical free–free, clamped–free, and clamped–clamped conditions emerge naturally as limiting cases. MATLAB is employed to extract the natural frequencies and mode shapes. Validation is performed through three-dimensional (3D) ANSYS simulations using quadratic HEX20 solid elements. The results demonstrate strong agreement between analytical and finite element predictions across a wide range of stiffness and mass parameters. Mesh convergence studies confirm stable and reliable solutions for the first six bending modes. The findings clearly illustrate that boundary flexibility and end inertia substantially influence modal characteristics and vibration behavior. In addition, the proposed formulation maintains analytical simplicity while capturing realistic structural behavior with high accuracy. The framework also provides a reliable benchmark for validating advanced numerical models and future experimental investigations. Overall, the proposed approach offers an accurate, computationally efficient, and practical tool for vibration prediction and engineering design of realistic beam structures.

Keywords: Euler-Bernoulli beam; free vibration; elastic boundary restraints; lumped end masses; modal analysis; finite element validation

1. Introduction

Beam vibration analysis remains a fundamental topic in structural and mechanical engineering because many practical components can be idealized as beam like structures. Classical beam theories provide accurate and elegant solutions for ideal boundary conditions. Real engineering systems, however, are far more complex. In practice, beams often interact with flexible supports, partial restraints, and attached components that significantly influence their dynamic response. As a result, increasing research attention has focused on incorporating elastic boundaries, end attachments, and realistic support conditions into vibration models while maintaining analytical clarity and computational efficiency.

Classical formulations based on Euler-Bernoulli and Timoshenko beam theories continue to provide a strong theoretical foundation for vibration analysis due to their physical transparency and practical applicability. Exact analytical beam solutions have been successfully applied to dynamic and adaptive structural problems while

preserving mathematical rigor [1]. Euler-Bernoulli beam models remain sufficiently accurate for many slender beam configurations and boundary conditions [2, 3]. Nevertheless, realistic effects such as coupled beam systems, variable geometry, and nonlinear support conditions can make the governing equations and eigenvalue formulations more complex. Coupled beam systems with elastic restraints have been investigated in previous studies [4]. Beam vibration with variable cross-sections has also received considerable attention [5]. Nonlinear end supports can further increase the complexity of vibration analysis [6]. For beams supported by elastic foundations, the foundation parameters can strongly influence structural stability [7]. In vibration problems, elastic foundations [8] and partially restrained supports [9] can significantly affect the natural frequencies and modal characteristics.

Related vibration studies have considered non-uniform elastic boundary constraints in cylindrical shells [10]. For beam systems, the combined influence of rotary inertia and elastic constraints has been examined for beams supported by elastic foundations [11]. Accurate vibration solutions for Timoshenko beams with general elastic support have also been reported [12]. More recently, elastically restrained cantilever Timoshenko beams with attached components have been investigated [13].

Attachments and lumped masses also play an important role in beam vibration. They can significantly change the natural frequencies and mode shapes. However, spring–mass systems and distributed attachments often lead to larger system matrices and more complicated frequency equations [14, 15]. As beam configurations become more complex, particularly in coupled systems, researchers increasingly rely on dynamic stiffness methods, optimization-based techniques, or computationally intensive finite element formulations to capture these interactions accurately [16-18]. Although these approaches provide reliable predictions, they often reduce analytical transparency and increase computational cost.

Numerical validation is equally important for assessing the accuracy and reliability of analytical vibration models. The choice of finite element type and mesh density can strongly influence the predicted frequencies and mode shapes, making convergence studies essential [19]. Small modeling variations, such as the treatment of mass matrices or attached components, may also produce noticeable differences in modal response [20, 21]. Consequently, vibration studies benefit greatly from frameworks that combine analytical clarity with systematic numerical validation. Such approaches improve confidence in the results while providing deeper physical insight into structural behavior [22]. Recent multi-fidelity studies on laminated CFRP beams further demonstrate the value of combining analytical prediction with 3D finite element validation and mesh-convergence assessment for reliable modal analysis [23].

Advanced formulations for composite and functionally graded beams have demonstrated very high accuracy in predicting vibration characteristics and eigenvalues [24-26]. This improved accuracy, however, is usually accompanied by increased mathematical complexity and higher computational effort. As a result, many existing methods become difficult to implement for practical engineering applications involving flexible supports and attached masses. These studies therefore highlight the continuing need for compact, transparent, and computationally efficient vibration formulations.

Recent investigations have further extended beam vibration analysis to systems with elastic restraints, nonlinear boundaries, and attached components. For instance, Timoshenko beam models with elastic springs and arbitrary boundary conditions have been studied using Ritz-based and energy methods, although these formulations

often become mathematically involved [27]. Similarly, iterative and decomposition-based approaches have been applied to beams with nonlinear or flexible boundaries, confirming the strong influence of support behavior on vibration response [28]. More recent studies on coupled beam systems and nonlinear connectors also demonstrate that boundary stiffness and end attachments can significantly modify modal characteristics [29]. Besides finite element analysis, other numerical methods can also be used for vibration problems. The Differential Quadrature Method evaluates derivatives at selected points and can produce accurate results with relatively few nodes [30]. Bézier-based methods offer another way to approximate structural response, especially for more complex models [31]. In the present study, MATLAB root finding is used because the characteristic equation is available in a compact form. ANSYS solid element simulations are then used for cross-verification and mesh-convergence assessment. Previous work has considered Bernoulli–Euler beams with point masses, rotary inertia, and elastic end restraints. An exact solution using translational and rotational springs at both beam ends [32]. The present study builds on this line of work by organizing translational stiffness, rotational stiffness, lumped end masses, and end rotary inertia within one compact (4×4) frequency dependent matrix.

Motivated by these observations, the present study develops a unified analytical framework for the eigenvalue analysis of uniform Euler Bernoulli beams with elastic supports and lumped end masses. The formulation incorporates translational stiffness, rotational stiffness, and discrete end inertia within a single consistent framework. Unlike many existing approaches that rely on large system matrices or computationally intensive procedures, the proposed method retains the physical transparency and simplicity of classical beam theory while providing a compact 4 × 4 characteristic matrix formulation. This enables efficient numerical implementation and straightforward evaluation of vibration characteristics under different support conditions.

The proposed framework is not intended to introduce new physical effects, since elastic restraints and end masses have been studied previously. Instead, the main contribution lies in integrating these coupled boundary and inertia effects into a concise and practically convenient analytical formulation. The method avoids treating different support conditions separately and provides a unified representation for free-free, clamped-free, and clamped-clamped configurations through appropriate stiffness parameters. Natural frequencies and mode shapes are obtained through MATLAB based eigenvalue computations, while validation is performed using 3D ANSYS simulations with detailed mesh convergence studies.

The results demonstrate that the formulation provides accurate and stable predictions over a broad range of stiffness and mass parameters. In addition to its computational efficiency, the framework offers a reliable benchmark for validating finite element models and future experimental investigations involving beam-like structures with non-ideal boundary conditions.

2. Materials and methods

The support conditions of real engineering beams are rarely as ideal as those assumed in textbooks. In practice, supports have finite translational and rotational stiffness, and end fittings such as sensors, brackets, connectors, or pads may introduce additional inertia. These effects can vary widely from one application to another. To include them while preserving analytical tractability, this study considers a uniform Euler–Bernoulli beam with elastic end restraints and concentrated end masses with

rotary inertia. The model represents a broad class of engineering components and experimental structures in which both boundary flexibility and point attachments influence the vibration behavior.

2.1. Problem Geometry and Physical Parameters

The mechanical model considered in this study is illustrated in **Figure 1**. A straight, uniform Euler Bernoulli beam of length L, bending rigidity EI, and mass per unit length ρ is examined. Both ends of the beam are supported by elastic restraints with discrete attachments. Translational springs restrict vertical displacement, while rotational springs oppose end rotation, resulting in partial constraints on displacement and slope. In addition, lumped masses with associated rotary inertia are attached at both ends. These end attachments represent practical components such as sensors, actuators, or end blocks commonly encountered in engineering structures.

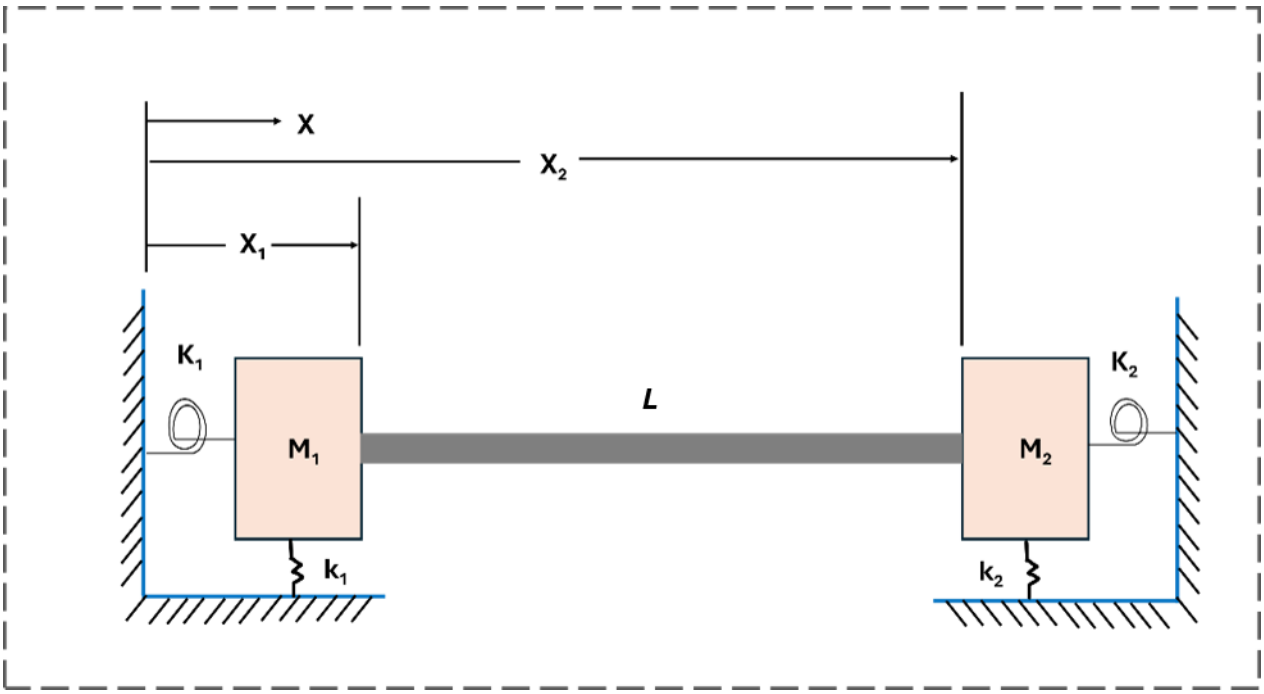


Figure 1. Beam with elastic end restraints and lumped masses (concept inspired by classical formulations presented in [33])

The transverse displacement of the beam is denoted by $w(x,t)$, and the corresponding slope is given by $\theta(x,t) = \partial w/\partial x$. Incorporation of elastic restraints and discrete inertia results in a shear bending moment coupling at the beam ends, which permits nonideal behavior at the supports to be accurately modeled while still obtaining an analytically tractable model. Classical boundary conditions like free-free, fixed-free and fixed-fixed are recovered as special cases by specifying appropriate stiffness and mass parameters.

Table 1. Nomenclature used in the present formulation

Symbol	Description
L	Length of the beam
EI	Bending rigidity of the beam
ρ	Mass per unit length

Continuation Table:

Symbol	Description
$w(x,t)$	Transverse displacement
$\phi(x)$	Mode shape function
ω	Natural angular frequency
α	Frequency parameter
k_1, k_2	Translational spring stiffness at the left and right ends
K_1, K_2	Rotational spring stiffness at the left and right ends
M_1, M_2	Lumped end masses
I_{M1}, I_{M2}	Rotary inertia of the left and right end masses, respectively
x	Axial coordinate along the beam
C_1, C_2, C_3, C_4	Constants in the mode shape solution
b_1, b_2	Width dimensions of rigid end masses $M_1$and M_2
f_n	Natural frequency in Hz
ω_n	Natural frequency in rad/sec

2.2. Free Vibration Assumption and Governing Relations

With the physical model established, the governing relations for free vibration are derived using classical Euler-Bernoulli beam theory. The model assumes small transverse deformation and bending-dominated behavior. It is most suitable for slender beams, where transverse shear deformation and beam rotary inertia have a limited influence on the vibration response. These effects are not included in the present formulation. Therefore, accuracy may decrease for less slender beams and at higher vibration modes, particularly for rectangular sections where 3D effects can become more important. For cases with lower slenderness ratios, such as ($L/D \approx 10$), these effects may influence the higher modes more strongly. Such cases are included to assess the practical applicability range of the formulation rather than to claim full thick-beam accuracy.

The bending moment $M(x,t)$ and shear force $V(x,t)$ are related to the transverse displacement $w(x,t)$ as,

$$M\left(x,t\right)=EI\frac{\partial^2 w\left(x,t\right)}{\partial x^2},V\left(x,t\right)=EI\frac{\partial^3 w\left(x,t\right)}{\partial x^3}.$$

Within the context of free vibration analysis, the transverse deflection is assumed to oscillate sinusoidally in time. Therefore, it can be written in a complex form such as,

$$w\left(x,t\right)=\phi\left(x\right)e^{i\omega t},$$

Where $\phi(x)$ denotes the spatial mode shape and ω is the natural angular frequency. This representation is mathematically equivalent to the real trigonometric form and is adopted here for analytical convenience. Substituting this expression into the governing relations, together with the definitions of bending moment and shear force, yields frequency dependent boundary conditions. That explicitly accounts for the effects of elastic restraints and lumped end masses.

2.3. Boundary Conditions for Beams with Discrete End Masses and Elastic supports

The beam is connected at both ends to elastic restraints and discrete rigid attachments. The left and right boundaries are located at $x = 0$ and $x = L$, respectively. At each end, translational springs resist transverse displacement, while rotational springs oppose end rotation. In addition, lumped end masses and their associated rotary inertia introduce inertia forces and moments under harmonic motion. These effects are incorporated by enforcing force and moment equilibrium between the internal beam actions and the boundary reactions at both ends.

The parameters $b_1$and b_2 denote the widths of the rigid end masses $M_1$and M_2, respectively, as illustrated in **Figure 2**.

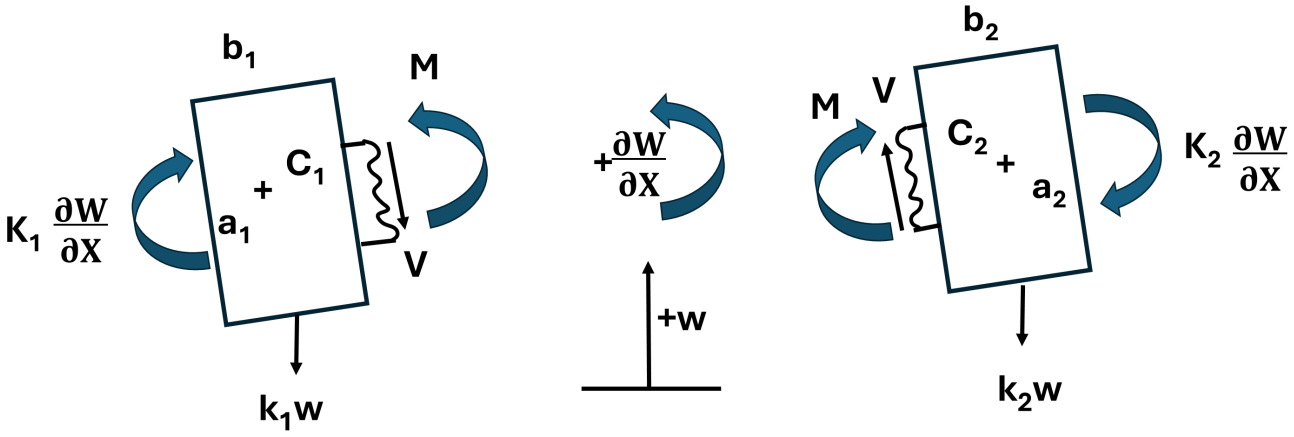


Figure 2. Free body diagram for the two end masses

$$\left.\begin{aligned} &EIX''' + \left(k_1 - M_1\omega^2\right)X = 0 && \text{(a)} \\ &EIX'' - \left[\frac{EIb_1}{2}\right]X''' - \left(K_1 - I_{M_1}\omega^2\right)X' = 0 && \text{(b)} \end{aligned}\right] \quad \text{(at x = } x_1\text{)} \tag{1}$$

$$\left.\begin{aligned} &EIX''' + \left(k_2 - M_2\omega^2\right)X = 0 && \text{(a)} \\ &EIX'' - \left[\frac{EIb_2}{2}\right]X''' - \left(K_2 - I_{M_2}\omega^2\right)X' = 0 && \text{(b)} \end{aligned}\right] \quad \text{(at x = } x_1\text{)} \tag{2}$$

The above relations comprehensively represent the combined influence of elastic end restraints and discrete end inertia on the beam behavior. In the limiting cases where the stiffness or inertia parameters tend toward zero or infinity, the formulation consistently reduces to classical boundary conditions. These frequency dependent boundary conditions establish a rigorous framework and form the basis for deriving the analytical solution of the associated eigenvalue problem in the following section

3. Analytical solution

In this section, the free vibration response of the beam is obtained through an analytical approach based on the separation of variables. The analysis begins with the general mode shape solution of the Euler–Bernoulli beam equation. The frequency dependent boundary conditions derived in Section 2.3 are then imposed on this solution. Enforcing these conditions results in a system of homogeneous algebraic equations, which is conveniently expressed in matrix form. The requirement for

a non-trivial solution leads to the characteristic equation, from which the natural frequencies of the system are determined.

3.1. Closed Form Mode Shape Solution

Using the method of separation of variables, the transverse displacement is expressed as the product of spatial and temporal functions. The spatial component satisfies the governing Euler-Bernoulli beam equation, leading to the classical analytical solution composed of trigonometric and hyperbolic terms.

$$X(x) = C_1 sin\alpha x + C_2 cos\alpha x + C_3 sinh\alpha x + C_4 cosh\alpha x \tag{3}$$

Where C_1, C_2, C_3, and C_4 are constant determined from the boundary conditions, while α represents the frequency parameter associated with the natural frequencies of the beam. The general solution is differentiated successively from first to third order to obtain the required slope, bending moment, and shear force expressions. The corresponding boundary conditions are then applied at $x = x_1 = 0$ (left end) and $x = x_2 = l$ (right end) according to the specified support constraints,

$$X(0) = C_2 + C_4 \tag{3a}$$

$$X(l) = C_1 sin\alpha l + C_2 cos\alpha l + C_3 sinh\alpha l + C_4 cosh\alpha l \tag{3b}$$

The first derivative of Eq. (3), representing the slope of the beam, is obtained as follows,

$$X'(x) = C_1 \alpha cos\alpha x - C_2 \alpha sin\alpha x + C_3 \alpha cosh\alpha x + C_4 \alpha sinh\alpha x \tag{3c}$$

$$X'(0) = C_1 \alpha + C_3 \alpha \tag{3d}$$

$$X'(l) = C_1 \alpha cos\alpha l - C_2 \alpha sin\alpha l + C_3 \alpha cosh\alpha l + C_4 \alpha sinh\alpha l \tag{3e}$$

The second derivative of Eq. (3), which is related to the bending moment, is obtained as follows,

$$X''(x) = -C_1 \alpha^2 sin\alpha x - C_2 \alpha^2 cos\alpha x + C_3 \alpha^2 sinh\alpha x + C_4 \alpha^2 cosh\alpha x \tag{3f}$$

$$X''(0) = -C_2 \alpha^2 + C_4 \alpha^2 \tag{3g}$$

$$X''(l) = -C_1 \alpha^2 sin\alpha l - C_2 \alpha^2 cos\alpha l + C_3 \alpha^2 sinh\alpha l + C_4 \alpha^2 cosh\alpha l \tag{3h}$$

The third derivative of Eq. (3), which is related to the shear force, is obtained as follows,

$$X'''(x) = -C_1 \alpha^3 cos\alpha x + C_2 \alpha^3 sin\alpha x + C_3 \alpha^3 cosh\alpha x + C_4 \alpha^3 sinh\alpha x \tag{3i}$$

$$X'''(0) = -C_1 \alpha^3 + C_3 \alpha^3 \tag{3j}$$

$$X'''(l) = -C_1 \alpha^3 cos\alpha l + C_2 \alpha^3 sin\alpha l + C_3 \alpha^3 cosh\alpha l + C_4 \alpha^3 sinh\alpha l \tag{3k}$$

Expressions from Eqs. (3a) to (3k) are then substituted into the boundary condition in Eq. (1a). For the left end, $x = x_1 = 0$, the translational and rotational stiffness terms are applied as follows,

$$EIX'''(0) + \left(k_1 - M_1\omega^2\right) X(0) = 0$$

$$EI\left(-C_1\alpha^3 + C_3\alpha^3\right) + \left(k_1 - M_1\omega^2\right)\left(C_2 + C_4\right) = 0 \tag{4}$$

After simplification and normalization by EI, Eq. (4) can be expressed in the following form,

$$\left(-\alpha^3\right) C_1 + \left[\frac{k_1 - M_1\omega^2}{EI}\right] C_2 + \left(\alpha^3\right) C_3 + \left[\frac{k_1 - M_1\omega^2}{EI}\right] C_4 = 0 \tag{5}$$

From the rotary inertia boundary condition given in Eq. (1b), the relation for the left end, $x = x_1 = 0$, is obtained as follows,

$$EIX''(0) - \left[\frac{EIb_1}{2}\right] X'''(0) - \left(K_1 - I_{M_1}\omega^2\right) X'(0) = 0$$

$$EI\left(-C_2\alpha^2 + C_4\alpha^2\right) - \left[\frac{EIb_1}{2}\right]\left(-C_1\alpha^3 + C_3\alpha^3\right) - \left(K_1 - I_{M_1}\omega^2\right)(C_1\alpha + C_3\alpha) = 0 \quad (6)$$

After simplification of Eq. (6) and normalization by the corresponding stiffness term, the final expression is obtained as follows,

$$\left[\frac{b_1}{2}\alpha^3 - \left(\frac{K_1 - I_{M_1}\omega^2}{EI}\,\alpha\right)\right] C_1 + \left(-\alpha^2\right) C_2 + \left[-\frac{b_1}{2}\alpha^3 - \left(\frac{K_1 - I_{M_1}\omega^2}{EI}\,\alpha\right)\right] C_3 + \left(\alpha^2\right) C_4 = 0 \quad (7)$$

From the boundary condition given in Eq. (2a), the relation at the right end of the beam, $x = x_2 = l$, is obtained and simplified as follows,

$$EIX'''(l) + \left(k_2 - M_2\omega^2\right) X(l) = 0$$

After substituting $X'''(l)$ and $X(l)$ into Eq. (2a), the right-end boundary condition is expressed in terms of the unknown constants C_1-C_4. This relation forms one row of the characteristic matrix. The nondimensional frequency parameter is defined as $\beta = \alpha l$. After normalization by EI, the equation can be written in its final matrix ready form,

$$\begin{aligned} &EI(-C_1\alpha^3 cos\alpha l - C_2\alpha^3 sin\alpha l + C_3\alpha^3 cosh\alpha l + C_4\alpha^3 sinh\alpha l) + \\ &\left(k_2 - M_2\omega^2\right)\left(\, C_1 sin\alpha l + C_2 cos\alpha l + C_3 sinh\alpha l + C_4 cosh\alpha l\right) = 0 \end{aligned} \quad (8)$$

After simplification of Eq. (8), the final expression is obtained as follows,

$$\left[-\alpha^3 cos\beta + \left(\frac{(k_2 - M_2\omega^2}{EI}\, sin\beta\right)\right] C_1 + \left[?\alpha^3 sin\beta + \left(\frac{k_2 - M_2\omega^2}{EI}\right)\cos\beta\right] C_2 +$$

$$\left[\alpha^3 cosh\beta + \left(\frac{(k_2 - M_2\omega^2}{EI}\, sinh\beta\right)\right] C_3 + \left[\alpha^3 sinh\beta + \left(\frac{(k_2 - M_2\omega^2}{EI}\, cosh\beta\right)\right] C_4 = 0 \quad (9)$$

From the boundary condition given in Eq. (2b) at the right end of the beam shown in **Figure 1**, the rotational equilibrium relation for $x = x_2 = l$ is simplified as follows,

$$EIX''(l) - \left[\frac{EIb_2}{2}\right] X'''(l) - \left(K_2 - I_{M_2}\omega^2\right) X'(l) = 0$$

After substituting $X'(l)$, $X''(l)$ and $X'''(l)$ into the above boundary condition, the simplified expression is obtained as follows,

$$\begin{aligned} &EI\left(-C_1\alpha^2 sin\beta - C_2\alpha^2 cos\beta + C_3\alpha^2 sinh\beta + C_4\alpha^2 cosh\beta\right) - \\ &\left[\frac{EIb_2}{2}\right](-C_1\alpha^3 cos\beta + C_2\alpha^3 sin\beta + C_3\alpha^3 cosh\beta + C_4\alpha^3 sinh\beta\ ) - \\ &\left(K_2 - I_{M_2}\omega^2\right)\left(C_1\alpha cos\beta - C_2\alpha sin\beta + C_3\alpha cosh\beta + C_4\alpha sinh\beta\ \right) = 0 \end{aligned} \quad (10)$$

After dividing the above equation by $EI\alpha$ and using $\beta = \alpha l$, the constants are separated. The final expression is obtained as follows,

$$\begin{aligned}
&\left[-\alpha sin\beta+\frac{b_2}{2}\alpha^2 cos\beta-\left(\frac{K_2-I_{M_2}\omega^2}{EI}\,cos\beta\right)\right]C_1+\\
&\left[-\alpha cos\beta-\frac{b_2}{2}\alpha^2 sin\beta+\left(\frac{K_2-I_{M_2}\omega^2}{EI}\,sin\beta\right)\right]C_2+\\
&\left[\alpha sinh\beta-\frac{b_2}{2}\alpha^2 cosh\beta-\left(\frac{K_2-I_{M_2}\omega^2}{EI}\,cosh\beta\right)\right]C_3+\\
&\left[\alpha cosh\beta-\frac{b_2}{2}\alpha^2 sinh\beta-\left(\frac{K_2-I_{M_2}\omega^2}{EI}\,sinh\beta\right)\right]C_4=0
\end{aligned} \tag{11}$$

3.2. Matrix Formulation of the Eigenvalue Problem

The boundary conditions derived in Section 2.3 are enforced by substituting the closed form mode shape solution and its corresponding derivatives, presented in Section 3.1, into the boundary relations at $x = 0$ and $x = l$. This procedure directly couples the displacement field with elastic supports stiffness and attached end masses. As a result, four homogeneous algebraic equations are obtained in terms of the unknown constants C_1, C_2, C_3, and C_4. These equations are then assembled into a compact matrix form,

$$\mathrm{K}(\alpha)\mathrm{C}=0,$$

Where,

$$\mathbf{C}=[C_1\ C_2\ C_3\ C_4]^T$$

is the vector of unknown coefficients, and $K(\alpha)$ is the frequency dependent coefficient matrix representing the combined influence of elastic boundary restraints and discrete end inertia on the dynamic response of the beam. A non trivial solution exists only when the determinant of the coefficient matrix becomes zero, leading to the characteristic equation,

$$\det\left[\mathrm{K}(\alpha)\right]=0.$$

Solving this equation yields the admissible eigenvalues of the system. The corresponding natural frequencies are then obtained for arbitrary combinations of boundary stiffness and end inertia, allowing a unified evaluation of the vibration behavior.

$$\begin{bmatrix}
(-\alpha^3) & \left(\frac{k_1-M_1\omega^2}{EI}\right) & (\alpha^3) & \left(\frac{k_1-M_1\omega^2}{EI}\right)\\
\frac{b_1}{2}\alpha^3-\left(\frac{K_1-I_{M_1}\omega^2}{EI}\,\alpha\right) & (-\alpha^2) & -\frac{b_1}{2}\alpha^3-\left(\frac{K_1-I_{M_1}\omega^2}{EI}\,\alpha\right) & (\alpha^2)\\
-\alpha^3 cos\beta+\left(\frac{(k_2-M_2\omega^2}{EI}\,sin\beta\right) & +\alpha^3 sin\beta+\left(\frac{(k_2-M_2\omega^2}{EI}\,cos\beta\right) & +\alpha^3 cosh\beta+\left(\frac{(k_2-M_2\omega^2}{EI}\,sinh\beta\right) & +\alpha^3 sinh\beta+\left(\frac{(k_2-M_2\omega^2}{EI}\,cosh\beta\right)\\
\alpha cosh\beta-\frac{b_2}{2}\alpha^2 sinh\beta-\left(\frac{K_2-I_{M_2}\omega^2}{EI}\,sinh\beta\right) & \alpha sinh\beta-\frac{b_2}{2}\alpha^2 cosh\beta-\left(\frac{K_2-I_{M_2}\omega^2}{EI}\,cosh\beta\right) & -\alpha cos\beta-\frac{b_2}{2}\alpha^2 sin\beta+\left(\frac{K_2-I_{M_2}\omega^2}{EI}\,sin\beta\right) & \alpha cosh\beta-\frac{b_2}{2}\alpha^2 sinh\beta-\left(\frac{K_2-I_{M_2}\omega^2}{EI}\,sinh\beta\right)
\end{bmatrix}$$

$$\begin{bmatrix}C_1\\C_2\\C_3\\C_4\end{bmatrix}=0$$

In practice, the determinant of the frequency dependent coefficient matrix is evaluated numerically as a function of the frequency parameter. The resulting

nonlinear characteristic equation is solved in MATLAB using root finding techniques to obtain the admissible eigenvalues. Although the mode shape expression is obtained in closed analytical form, the natural frequencies are determined numerically from the characteristic determinant. Once the eigenvalues are identified, the corresponding mode shapes are evaluated by substituting the constants back into the matrix equation up to a normalization factor.

4. Results and discussion

The results are organized to first verify the proposed analytical formulation against classical reference solutions and then evaluate its accuracy through 3D finite element validation and mesh convergence studies. The analytical characteristic equations are solved numerically in MATLAB in terms of the nondimensional frequency parameter β and the natural frequency f_n. Although the mode shape solution is obtained analytically, the eigenvalues are extracted numerically from the frequency dependent determinant characteristic. The analytical results were cross verified using ANSYS Workbench 2023 R2. The beam models were analyzed using quadratic HEX20 solid elements based on full 3D elasticity theory. Because the analytical model follows Euler–Bernoulli beam theory, whereas the ANSYS model includes transverse shear, Poisson, and other 3D effects, the ANSYS results are used as an independent benchmark rather than an absolute reference solution. The comparison assesses the applicability and engineering accuracy of the proposed compact 4 × 4 framework. Mesh refinement was performed to ensure convergence of the finite-element results. The remaining differences, particularly in higher modes, are attributed to the different assumptions of the one-dimensional analytical and 3D numerical models. All simulations were conducted under identical computational conditions to ensure consistency and reproducibility.

In the result tables, Book refers to the classical reference solutions reported by Leissa and Qatu [33]. MATLAB denotes the numerical implementation of the present analytical formulation, while ANSYS (HEX20) represents 3D finite element predictions. For all simulations, aluminum is selected as the representative material with Young's modulus E = 70×10^9 Pa and Poisson's ratio ν = 0.33. Circular and rectangular beams with a length of L = 1 m are analyzed under free-free (FF), clamped-free (CF), and clamped-clamped (CC) boundary conditions. These support conditions are modeled through appropriate selections of translational and rotational stiffness parameters k and K. For the FF configuration, k = 0 and K = 0, resulting in rigid body modes for the first two frequencies. The CF and CC conditions are obtained by assigning sufficiently large stiffness values at the restrained boundaries. Circular beams with diameters of 0.10 m and 0.05 m, together with rectangular beams of cross-sections 0.06 m×0.12 m and 0.03 m×0.06 m, are considered to investigate the influence of geometry and boundary stiffness on the vibration response. The following subsections present the validation results, convergence behavior, and modal characteristics obtained using the proposed formulation.

4.1. Numerical Implementation and Mesh Convergence for Circular Beams

Circular beams are modeled using quadratic 20 node hexahedral (HEX20) solid elements based on full 3D elasticity theory. This element type is well suited for bending dominated vibration problems and provides reliable prediction of modal characteristics. A mesh convergence study is conducted to ensure that the computed natural frequencies are sufficiently independent of discretization. Several mesh

sizes are examined, and the first six bending modes are monitored. The frequency variations decrease progressively with mesh refinement, confirming stable numerical convergence.

As expected, computational cost increases with mesh refinement. Coarse meshes require only a short solution time, whereas simulations with an element size of 0.005 m typically require approximately 1-2 minutes, including meshing and solution stages. Further refinement to 0.001 m substantially increases the number of elements and computational time, reaching nearly two hours per simulation case, while providing only marginal improvement in the predicted frequencies. Based on this accuracy efficiency balance, an element size of 0.005 m is selected for the circular-beam simulations. This mesh characteristics in **Table 2**, provides stable and computationally efficient results suitable for validating the proposed analytical framework.

Table 2. Finite element mesh characteristics for circular beam models discretized using quadratic 20-node hexahedral (HEX20) solid elements based on 3D elasticity theory

Diameter (m)	Element Size (m)	Number of Elements	Number of Nodes
0.1	Default	80	621
0.1	0.02	1,450	7,204
0.1	0.015	3,886	18,289
0.1	0.01	9,700	44,124
0.1	0.005	77,200	329,623
0.05	0.005	19,400	87,924
0.05	0.001	2,285,000	9,389,016

4.2 Modal Analysis and Mesh Convergence of Circular Beams

This section presents the modal analysis results for solid circular beams using the proposed analytical formulation based on Classical Beam Theory (CBT). Reference solutions reported by Leissa and Qatu [33] are used for validation. The frequency equations are solved numerically in MATLAB, while ANSYS HEX20 simulations are performed to evaluate numerical accuracy and mesh convergence. Circular beams with diameters of 0.10 m and 0.05 m are analyzed under FF, CF, and CC boundary conditions.

4.2.1 Circular Beam (D = 0.1 m)

Tables 3-8 present the nondimensional frequency parameters and natural frequencies for circular beams under FF, CF, and CC boundary conditions. The results compare classical reference solutions, MATLAB predictions from the present formulation, and 3D ANSYS simulations. These comparisons provide a consistent evaluation of the proposed analytical framework and the convergence behavior of the numerical models.

Free-Free Boundary Condition

For the FF circular beam, the first two modes correspond to rigid body translation and rotation and therefore exhibit zero natural frequencies. The higher modes represent flexural bending behavior and are used for comparison. The

nondimensional frequency parameters listed in Table 3 shows exact agreement between the classical reference solutions and the MATLAB results, confirming the correctness of the analytical implementation. The angular frequencies reported in **Table 4** show that the ANSYS HEX20 results approach the analytical predictions as the mesh is refined. For finer meshes, the frequency variations become very small, indicating stable and mesh-independent numerical behavior.

Table 3. Comparison of non-dimensional frequency parameters (β^2) for a free-free circular beam between classical reference solutions [33] and the present analytical formulation

Mode (m)	β^2	β^2 (CBT) (MATLAB)
1.0	0.0	0.0
2.0	0.0	0.0
3.0	22.4	22.4
4.0	61.7	61.7
5.0	120.9	120.9
6.0	199.7	199.9

Table 4. Angular natural frequencies of a free-free (FF) circular beam obtained from analytical and ANSYS simulations

Mode (m)	f_n (Hz) CBT (MATLAB)	f_n (Hz) HEX20 (3D) Default	f_n (Hz) HEX20 (3D) 0.02 m	f_n (Hz) HEX20 (3D) 0.015 m	f_n (Hz) HEX20 (3D) 0.01 m	f_n (Hz) HEX20 (3D) 0.005 m
1	0.0	0.0	0.0	0.0	0.0	0.0
2	0.0	0.0	0.0	0.0	0.0	0.0
3	2846.5	2773.8	2776.3	2776.4	2776.5	2776.5
4	7846.9	7333.1	7331.2	7331.8	7331.8	7331.9
5	15382.2	13970.4	13985.7	13986.0	13986.9	13987.0
6	25427.7	23400.6	23424.2	23425.3	23427.2	23427.7

Clamped-Free (Fixed-Free) Boundary Condition

For the CF circular beam, rigid-body motion is suppressed by the clamped boundary, resulting in nonzero natural frequencies for all modes. The nondimensional frequency parameters β^2 listed in **Table 5** show close agreement between the classical reference solutions and the MATLAB results, confirming the correctness of the analytical implementation. The natural frequencies f_n reported in **Table 6** compare the analytical predictions with ANSYS HEX20 simulations. Small discrepancies appear for coarse meshes, particularly in higher modes, although these differences decrease progressively with mesh refinement. For refined meshes, the frequencies stabilize and show acceptable agreement with the analytical predictions considering the assumptions of Euler–Bernoulli beam theory.

Table 5. Comparison of non-dimensional frequency parameters (β^2) for a clamped– free circular beam between reference solutions [33] and the present analytical formulation

Mode (m)	β^2	β^2 (CBT) (MATLAB)
1	3.5	3.5

Continuation Table:

Mode (m)	β^2	β^2 (CBT) (MATLAB)
2	22.0	22.0
3	61.7	61.7
4	120.9	120.9
5	199.9	199.9
6	298.3	298.6

Table 6. Angular natural frequencies of a clamped–free circular beam predicted by the analytical model and validated using ANSYS (HEX20) simulations with mesh refinement

Mode (m)	f_n (Hz) CBT (MATLAB)	f_n (Hz) HEX20 (3D) Default	f_n (Hz) HEX20 (3D) 0.02 m	f_n (Hz) HEX20 (3D) 0.015 m	f_n (Hz) HEX20 (3D) 0.01 m	f_n (Hz) HEX20 (3D) 0.005 m
1	447.3	444.3	444.4	444.5	444.5	444.6
2	2803.5	2720.9	2724.0	2724.4	2725.0	2725.5
3	7850.0	7025.1	7028.5	7029.9	7030.2	7030.7
4	15382.2	14244.1	14255.1	14256.2	14257.1	14257.2
5	25427.7	23572.9	23581.5	23582.5	23583.9	23684.0
6	37985.2	35565.3	35574.7	35575.4	35575.6	35575.8

Clamped-Clamped (Fixed-Fixed) Boundary Condition

For the CC circular beam, both displacement and rotation are restrained at the beam ends, resulting in the highest natural frequencies among the boundary conditions considered. The nondimensional frequency parameters β^2 reported in **Table 7** show close agreement between the classical reference solutions and the MATLAB predictions, indicating accurate implementation of the boundary conditions. The natural frequencies f_n presented in **Table 8** compare the analytical predictions with ANSYS HEX20 simulations. Small discrepancies are observed for coarse meshes and higher modes, although these differences decrease with mesh refinement. For the refined meshes, the numerical results become stable and show acceptable agreement with the analytical predictions within the assumptions of Euler–Bernoulli beam theory.

Table 7. Non-dimensional frequency parameters (β^2) for a clamped–clamped circular beam, showing agreement between classical reference values [33] and the present analytical formulation

Mode (m)	β^2	β^2 (CBT) (MATLAB)
1	22.4	22.4
2	61.7	61.7
3	120.9	120.9
4	199.9	199.9
5	298.6	298.6
6	416.6	417.0

Table 8. Angular natural frequencies of a clamped–clamped circular beam obtained from the analytical solution and converged ANSYS (HEX20) results through mesh refinement

Mode (m)	f_n (Hz) CBT (MATLAB)	f_n (Hz) HEX20 (3D) Default	f_n (Hz) HEX20 (3D) 0.02 m	f_n (Hz) HEX20 (3D) 0.015 m	f_n (Hz) HEX20 (3D) 0.01 m	f_n (Hz) HEX20 (3D) 0.005 m
1	2846.5	2761.9	2773.8	2774.0	2774.5	2774.9
2	7846.9	7207.4	7224.2	7225.0	7227.1	7227.3
3	15382.2	14250.1	14259.6	14260.5	14261.6	14261.9
4	25427.7	23716.0	23724.2	23725.2	23726.3	23726.6
5	37985.2	34094.7	34102.2	34103.2	34104.2	34104.8
6	53053.4	46156.3	46164.5	46165.4	46166.8	46167.0

Figure 3 shows good agreement between the CBT and ANSYS HEX20 results for the FF, CF, and CC boundary conditions. Small deviations appear in higher modes, particularly for the more constrained cases. The natural frequencies increase progressively from FF to CF and reach the highest values for the CC condition due to the increase in boundary stiffness. These trends confirm the strong influence of support restraints on the modal response and demonstrate the applicability of the proposed analytical framework.

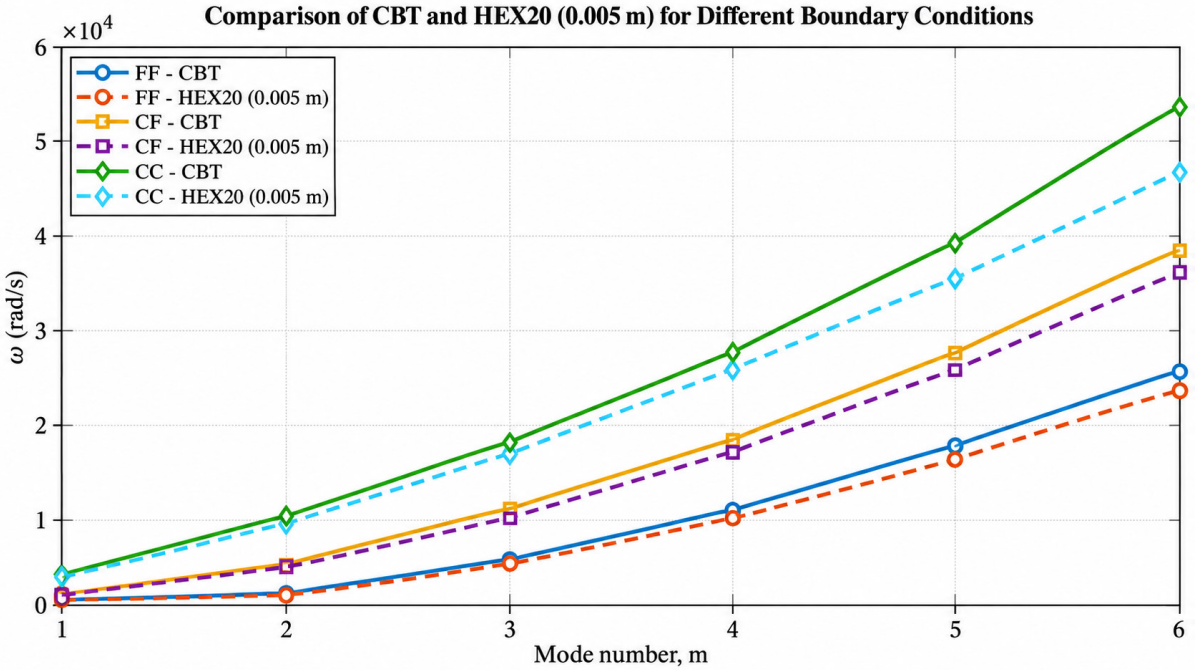


Figure 3. Comparison of CBT and ANSYS HEX20 results for circular beams (D = 0.10 m) under FF, CF, and CC boundary conditions.

4.2.2 Circular Beam (D = 0.05 m)

Tables 9-11 present the angular natural frequencies of the reduced-diameter circular beam for FF, CF, and CC boundary conditions, highlighting the influence of beam diameter on the modal response.

Free-Free Boundary Condition

For the FF circular beam with reduced diameter, the first two modes correspond

to rigid-body motion and therefore exhibit zero natural frequencies. The higher modes represent flexural bending behavior and are used for comparison. The ANSYS HEX20 results show good agreement with the analytical predictions, while the refined meshes produce stable frequencies for the higher modes.

Table 9. Angular natural frequencies of a free–free circular beam (D = 0.05 m) obtained from the analytical solution and ANSYS simulations with mesh refinement

Mode (m)	f_n (Hz) CBT (MATLAB)	f_n (Hz) HEX20 (3D) 0.005 m	f_n (Hz) HEX20 (3D) 0.001 m
1	0.0	0.0	0.0
2	0.0	0.0	0.0
3	1424.0	1415.2	1415.7
4	3925.3	3854.2	3854.7
5	7695.1	7430.3	7430.8
6	12720.0	12026.0	12026.9

Clamped-Free (Fixed-Free) Boundary Condition

For the CF circular beam, all vibration modes exhibit nonzero natural frequencies due to the clamped boundary condition. The ANSYS HEX20 results in **Table 10** shows good agreement with the analytical predictions, and the frequencies become stable with mesh refinement across all modes.

Table 10. Angular natural frequencies of a clamped–free circular beam (D = 0.05 m) predicted analytically and verified using ANSYS (HEX20) simulations under mesh refinement

Mode (m)	f_n (Hz) CBT (MATLAB)	f_n (Hz) HEX20 (3D) 0.005 m	f_n (Hz) HEX20 (3D) 0.001 m
1	223.8	223.6	223.6
2	1402.4	1392.1	1392.4
3	3926.8	3847.6	3848.0
4	7695.0	7399.4	7399.9
5	12720.0	11955.0	11955.7
6	19002.0	17402.0	17402.9

Clamped–Clamped (Fixed-Fixed) Boundary Condition

For the CC circular beam, full restraint at both ends produces the highest natural frequencies among the boundary conditions considered. The ANSYS HEX20 results in **Table 11** show good agreement with the analytical predictions, while the refined meshes provide stable and mesh-independent frequency values across all modes.

Table 11. Angular natural frequencies of a clamped–clamped circular beam (D = 0.05 m) obtained from the analytical formulation and corresponding ANSYS simulations with refined meshes

Mode (m)	f_n (Hz) CBT (MATLAB)	f_n (Hz) HEX20 (3D) 0.005 m	f_n (Hz) HEX20 (3D) 0.001 m
1	1424.0	1413.6	1413.7

Continuation Table:

Mode (m)	f_n (Hz) CBT (MATLAB)	f_n (Hz) HEX20 (3D) 0.005 m	f_n (Hz) HEX20 (3D) 0.001 m
2	3925.3	3836.1	3836.3
3	7695.1	7370.2	7370.4
4	12720.0	11890.9	11891.2
5	19002.0	18700.1	18700.6
6	26540.0	25001.5	25001.7

Figure 4 shows good agreement between the CBT and ANSYS HEX20 results for the refined meshes, indicating stable numerical convergence. The CC condition produces the highest frequencies, followed by CF and FF, due to the increase in boundary restraint stiffness. Small deviations appear in the higher modes, although the overall trends remain consistent. These results demonstrate the applicability of the proposed analytical framework for predicting the modal behavior of circular beam structures.

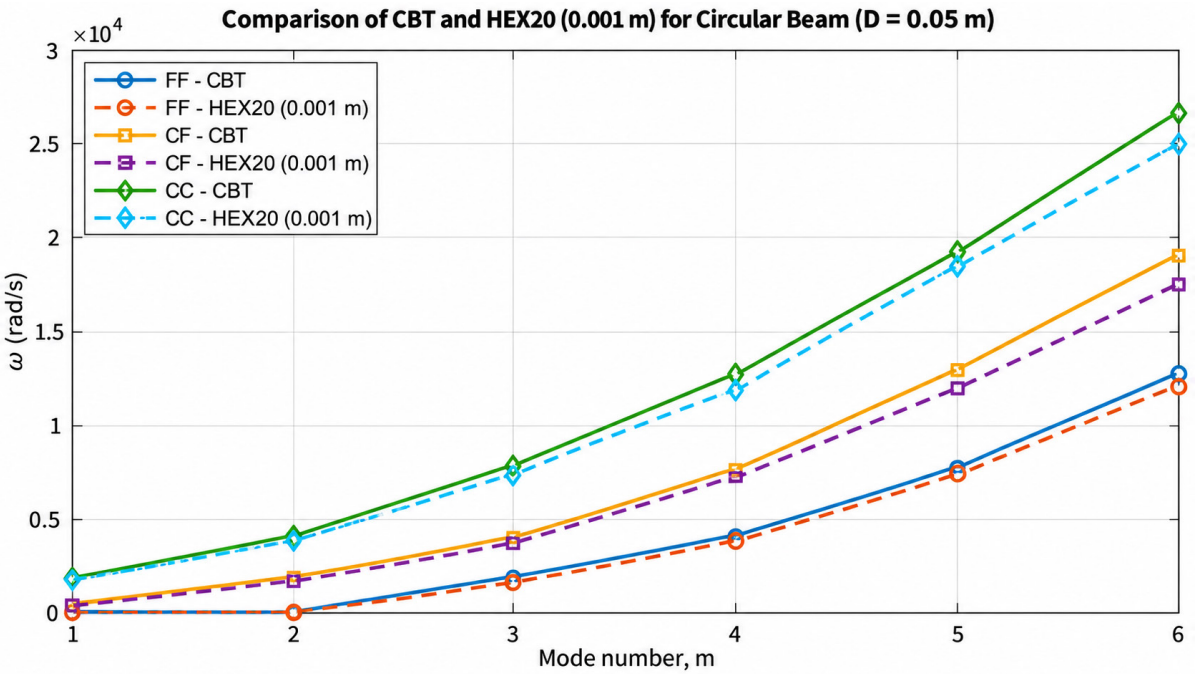


Figure 4. Comparison of CBT and ANSYS HEX20 results for circular beams (D=0.05 m) under FF, CF, and CC boundary conditions.

4.2.3 Mesh Convergence and Normalized Discretization (Circular Beams)

Mesh convergence is examined to ensure that the numerical results are sufficiently independent of discretization and suitable for cross verification of the proposed analytical framework. The study is performed for the CF boundary condition because this configuration produces higher curvature near the clamped end and is therefore more sensitive to mesh density. Once convergence is established for the CF case, the same discretization is considered adequate for the FF and CC configurations, which exhibit comparatively lower sensitivity. The selected mesh was also checked for all six bending modes to confirm stable numerical behavior over the frequency range considered.

To allow consistent comparison across different beam diameters, the mesh density is characterized using the normalized element size (h/D) rather than the absolute element size (h). Mode 3 was selected as a representative convergence indicator because it has sufficient curvature to show sensitivity to mesh refinement, whereas the lower modes converge more rapidly. However, Mode 3 was not used as the only convergence criterion. The frequencies of all six bending modes were examined at each mesh level. The higher mode ANSYS frequencies also became stable with further mesh refinement. Therefore, the remaining differences between the analytical and numerical results are mainly associated with the different assumptions of the Euler Bernoulli and 3D solid models, rather than insufficient mesh density. As shown in **Table 12**, reducing (h/D) results in only small changes in the Mode-3 frequency, indicating stable numerical convergence and four-digit accuracy. The selected mesh therefore provides an efficient and mesh-independent solution, while further refinement substantially increases computational cost with only marginal improvement in accuracy.

Table 12. Effect of normalized element size (h/D) on the third bending-mode frequency of circular beams under clamped–free boundary conditions.

D **(m)**	**BC**	***h*** **(m)**	***h/D***	**Mode-3** f_n **(Hz)**	Δf_n **(%)**
0.10	CF	0.01	0.10	7030.2	-
0.10	CF	0.005	0.05	7030.7	0.007
0.05	CF	0.005	0.10	3847.6	-
0.05	CF	0.001	0.02	3848.0	0.010

The graphs in **Figure 5** show only small variations in the third-mode frequency with mesh refinement, indicating stable convergence and mesh-independent numerical behavior. The convergence trend confirms that the selected discretization is sufficient to capture the dominant bending response with reliable accuracy. Monitoring the higher modes alongside Mode 3 further supports the overall stability of the numerical formulation. The selected mesh therefore provides an effective balance between computational efficiency and solution reliability for the circular beam models considered in this study.

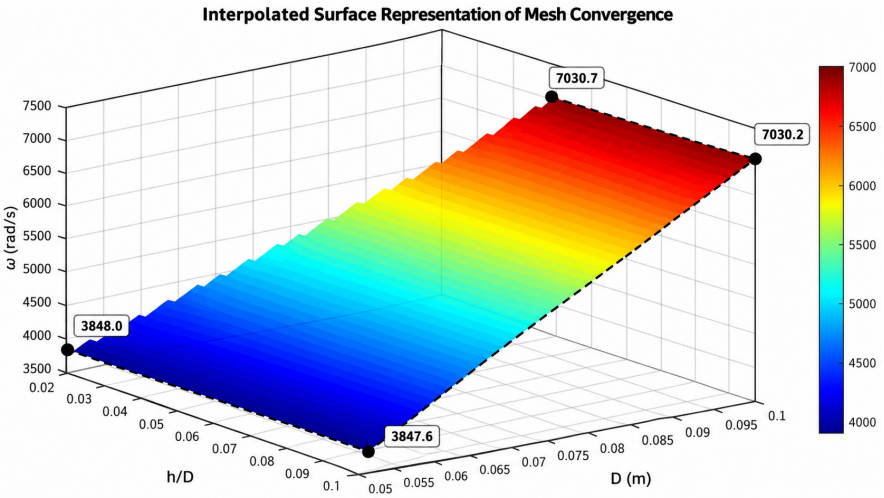


Figure 5. Interpolated surface plot showing the variation of the third bending-mode frequency with normalized mesh size (h/D) for circular beams under clamped–free boundary conditions.

4.3. Modal Analysis and Mesh Convergence of Rectangular Beams

These rectangular beam models were analyzed using quadratic 20-node hexahedral (HEX20) solid elements based on 3D elasticity theory. The objective was to identify a mesh that provides stable natural frequencies without excessive computational cost. A mesh-convergence study was performed by monitoring the first six vibration modes for rectangular cross-sections of (0.06,m×0.12,m)and (0.03,m×0.06,m).These cases also help assess the applicability range of the present Euler Bernoulli formulation. The rectangular sections have a relatively large bending depth compared with the beam length, especially for the (0.06,m×0.12,m) beam. Therefore, transverse shear deformation, beam rotary inertia, and other 3D effects can become more important, particularly at higher modes. The comparison with the ANSYS solid model is therefore treated as cross-verification of the analytical results, rather than strict validation for thick-beam behavior.

As the mesh was refined, the changes in the computed frequencies became smaller, indicating stable numerical convergence. Coarser meshes gave acceptable results for the lower modes but showed greater sensitivity in the higher modes. An element size of (0.005,m)produced stable and mesh-independent results for both geometries. Further refinement to (0.001,m) greatly increase the computational cost, with only small changes in the predicted frequencies. The selected mesh therefore provided a practical balance between numerical reliability and computational efficiency. The mesh characteristics are summarized in **Table 13**, while **Tables 14-19** present the analytical and finite-element results for the FF, CF, and CC boundary conditions.

Table 13. Finite element mesh information for rectangular beam models discretized using quadratic HEX20 solid elements.

Cross-Section (m^2)	Element Size (m)	Number of Elements	Number of Nodes
0.06 × 0.12	Default	120	849
0.06 × 0.12	0.02	900	5,123
0.06 × 0.12	0.015	2,144	11,243
0.06 × 0.12	0.01	7,200	34,653
0.06 × 0.12	0.005	57,600	253,337
0.03 × 0.06	0.005	14,400	69,053
0.03 × 0.06	0.001	1,800,000	7,477,581

4.3.1. Rectangular Beam (0.06 m × 0.12 m)

Tables 14-16 present the angular natural frequencies for the rectangular beam with cross-section 0.06 m×0.12 m under FF, CF, and CC boundary conditions. The analytical predictions are compared with 3D ANSYS simulations to evaluate the applicability of the proposed formulation. The results show good agreement for the lower and intermediate modes, while the refined meshes produce stable and mesh-independent frequency values.

Free-Free Boundary Condition

For the FF rectangular beam, the first two vibration modes correspond to rigid body translation and rotation and therefore exhibit zero natural frequencies. The higher modes represent flexural bending behavior and are used for

comparison. The angular frequencies reported in **Table 14** show good agreement between the analytical predictions and the ANSYS results for the lower and intermediate modes. As the mesh is refined, the finite element frequencies gradually stabilize, indicating mesh-independent numerical behavior for the FF rectangular beam configuration.

Table 14. Angular natural frequencies of a free–free rectangular beam (0.06 m × 0.12 m) obtained from the analytical solution and ANSYS simulations with mesh refinement

Mode (m)	f_n (Hz) CBT (MATLAB)	f_n (Hz) HEX20 (3D) Default	f_n (Hz) HEX20 (3D) 0.02 m	f_n (Hz) HEX20 (3D) 0.015 m	f_n (Hz) HEX20 (3D) 0.01 m	f_n (Hz) HEX20 (3D) 0.005 m
1	0.0	0.0	0.0	0.0	0.0	0.0
2	0.0	0.0	0.0	0.0	0.0	0.0
3	3946.3	3759.1	3765.0	3765.3	3765.6	3766.0
4	10878.0	10001.5	10008.6	10008.8	10009.6	10009.8
5	21325.0	20466.0	20474.9	20475.8	20476.1	20476.6
6	35252.0	29426.8	29433.6	29433.7	29434.1	29434.5

Clamped-Free (Fixed-Free) Boundary Condition

For the CF rectangular beam, rigid body motion is suppressed by the clamped boundary, resulting in nonzero natural frequencies for all modes. The ANSYS predictions show good agreement with the analytical results, particularly for the lower and intermediate modes. The frequency differences observed for coarse meshes decrease progressively with mesh refinement, leading to stable numerical behavior for the refined discretization.

Table 15. Angular natural frequencies of a clamped-free rectangular beam (0.06 m × 0.12 m) predicted by the analytical formulation and compared with ANSYS results under mesh refinement

Mode (m)	f_n (Hz) CBT (MATLAB)	f_n (Hz) HEX20 (3D) Default	f_n (Hz) HEX20 (3D) 0.02 m	f_n (Hz) HEX20 (3D) 0.015 m	f_n (Hz) HEX20 (3D) 0.01 m	f_n (Hz) HEX20 (3D) 0.005 m
1	620.2	616.3	616.5	616.7	616.9	616.9
2	3886.5	3679.1	3682.1	3683.2	3683.6	3683.6
3	10882.0	10086.1	10144.7	10147.2	10150.3	10154.1
4	21325.0	20610.8	20618.2	20619.8	20620.2	20620.8
5	35252.0	33755.8	33764.6	33765.4	33766.0	33766.7
6	52660.0	47213.2	47221.8	47222.1	47222.5	47222.7

Clamped-Clamped (Fixed-Fixed) Boundary Condition

For the CC rectangular beam, full restraint at both ends produces higher natural frequencies than the FF and CF configurations. The ANSYS results show good agreement with the analytical predictions for the lower and intermediate modes. With mesh refinement, in **Table 16**, the numerical frequencies become stable and exhibit mesh independent behavior across all modes considered.

Table 16. Angular natural frequencies of a clamped-clamped rectangular beam (0.06 m × 0.12 m) obtained from analytical predictions and 3D finite element simulations

Mode (m)	f_n (Hz) CBT (MATLAB)	f_n (Hz) HEX20 (3D) Default	f_n (Hz) HEX20 (3D) 0.02 m	f_n (Hz) HEX20 (3D) 0.015 m	f_n (Hz) HEX20 (3D) 0.01 m	f_n (Hz) HEX20 (3D) 0.005 m
1	3946.3	3647.3	3651.4	3651.7	3652.0	3652.2
2	10878.0	9984.8	9996.2	9998.0	9998.3	9998.4
3	21325.0	20381.7	20395.1	20396.6	20397.4	20397.5
4	35252.0	32141.2	32151.2	32152.1	32153.0	32153.2
5	52660.0	48123.9	48134.3	48135.3	48136.1	48136.5
6	73550.0	65124.7	65138.5	65140.0	65140.2	65140.7

Figure 6 shows consistent trends between the CBT and ANSYS HEX20 results for the FF, CF, and CC boundary conditions. Slightly larger deviations appear in higher modes compared with the circular beam cases, reflecting the increased influence of 3D effects in rectangular geometries. The CC condition produces the highest frequencies due to the stronger boundary restraint. Despite these differences, the overall modal trends remain consistent, demonstrating the applicability of the proposed analytical framework for rectangular beam vibration analysis. The analytical and ANSYS results differ because the two models use different assumptions. The analytical model is based on Euler–Bernoulli beam theory. It does not include transverse shear deformation, rotary inertia of the beam, cross-sectional warping, or Poisson effects. In contrast, the ANSYS HEX20 model is based on full 3D elasticity and includes these effects. Therefore, some difference is expected, especially for higher modes and rectangular beams. The ANSYS results are therefore used for cross-verification and to assess engineering accuracy, rather than as an absolute validation reference for the one-dimensional analytical model.

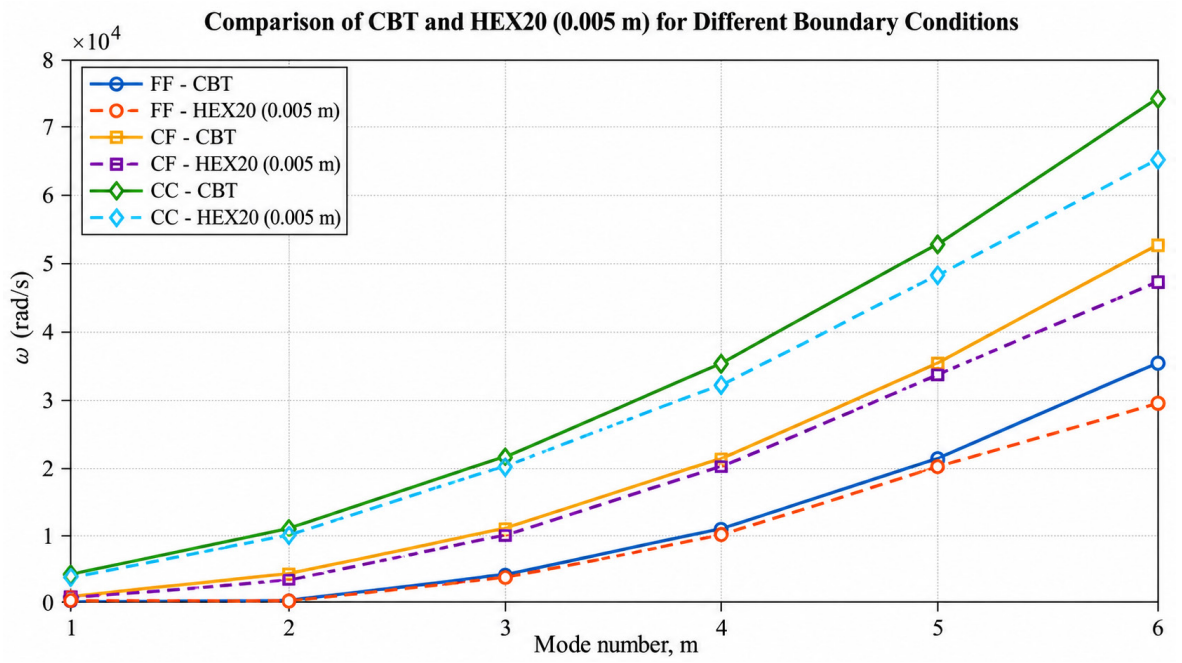


Figure 6. Comparison of CBT and ANSYS HEX20 results for rectangular beams (0.06×0.12 m) under FF, CF, and CC boundary conditions.

4.3.2. Rectangular Beam (0.03m × 0.06m)

Tables 17-19 present the angular natural frequencies for the rectangular beam with cross-section 0.03 m×0.06 m under FF, CF, and CC boundary conditions. The analytical predictions are compared with the ANSYS HEX20 results to evaluate the proposed formulation. Good agreement is observed for the lower and intermediate modes, while the refined meshes produce stable and mesh-independent frequency values across all boundary conditions.

Free-Free Boundary Condition

For the FF rectangular beam with reduced cross-section, the first two modes correspond to rigid body motion and therefore exhibit zero natural frequencies. The higher modes represent flexural bending behavior and are used for comparison. The ANSYS HEX20 results show good agreement with the analytical predictions for the lower and intermediate modes, while the selected mesh provides stable and mesh-independent frequency values.

Table 17. Angular natural frequencies of a free–free rectangular beam (0.03 m × 0.06 m) obtained from the analytical solution and ANSYS simulations with refined meshes

Mode (m)	f_n (Hz) CBT (MATLAB)	f_n (Hz) HEX20 (3D) 0.005 m	f_n (Hz) HEX20 (3D) 0.001 m
1	0.0	0.0	0.0
2	0.0	0.0	0.0
3	1973.1	1948.7	1949.0
4	5439.0	5248.8	5249.1
5	10663.0	9973.9	9974.1
6	17626.0	17387.5	17387.9

Clamped-Free (Fixed-Free) Boundary Condition

For the CF configuration, rigid-body motion is suppressed by the clamped boundary, resulting in nonzero natural frequencies for all modes. The ANSYS HEX20 results show good agreement with the analytical predictions, particularly for the lower and intermediate modes. The selected mesh produces stable frequency values with only small variations across the modes considered.

Table 18. Angular natural frequencies of a clamped–free rectangular beam (0.03 m × 0.06 m) obtained from analytical predictions and ANSYS validation under mesh refinement

Mode (m)	f_n (Hz) CBT (MATLAB)	f_n (Hz) HEX20 (3D) 0.005 m	f_n (Hz) HEX20 (3D) 0.001 m
1	310.1	309.9	310.0
2	1943.3	1909.8	1910.0
3	5441.2	5238.2	5238.8
4	10663.0	10974.8	10974.9
5	17626.0	17327.1	17327.4
6	26330.0	25671.2	25671.9

Clamped-Clamped (Fixed-Fixed) Boundary Condition

For the CC rectangular beam, full restraint at both ends produces the highest natural frequencies among the boundary conditions considered. The ANSYS HEX20 results show good agreement with the analytical predictions for the lower and intermediate modes. The computed frequencies remain stable for the selected mesh, indicating mesh-independent numerical behavior for the CC configuration.

Table 19. Angular natural frequencies of a clamped-clamped rectangular beam (0.03 m × 0.06 m) comparing analytical results with ANSYS simulations using refined meshes

Mode (m)	f_n (Hz) CBT (MATLAB)	f_n (Hz) HEX20 (3D) 0.005 m	f_n (Hz) HEX20 (3D) 0.001 m
1	1973.1	1934.0	1934.3
2	5439.0	5235.8	5236.0
3	10663.0	9772.2	9772.8
4	17626.0	17269.3	17269.9
5	26330.0	25416.3	25416.9
6	36775.0	32073.8	32074.0

Figure 7 shows consistent modal trends between the CBT and ANSYS HEX20 results as the mesh is refined. The frequency variation for the FF, CF, and CC boundary conditions remains physically consistent, with increasing restraint leading to higher natural frequencies. Small deviations appear mainly in higher modes due to 3D effects and discretization sensitivity. Overall, the results demonstrate stable numerical convergence and support the applicability of the proposed analytical framework for rectangular beam vibration analysis.

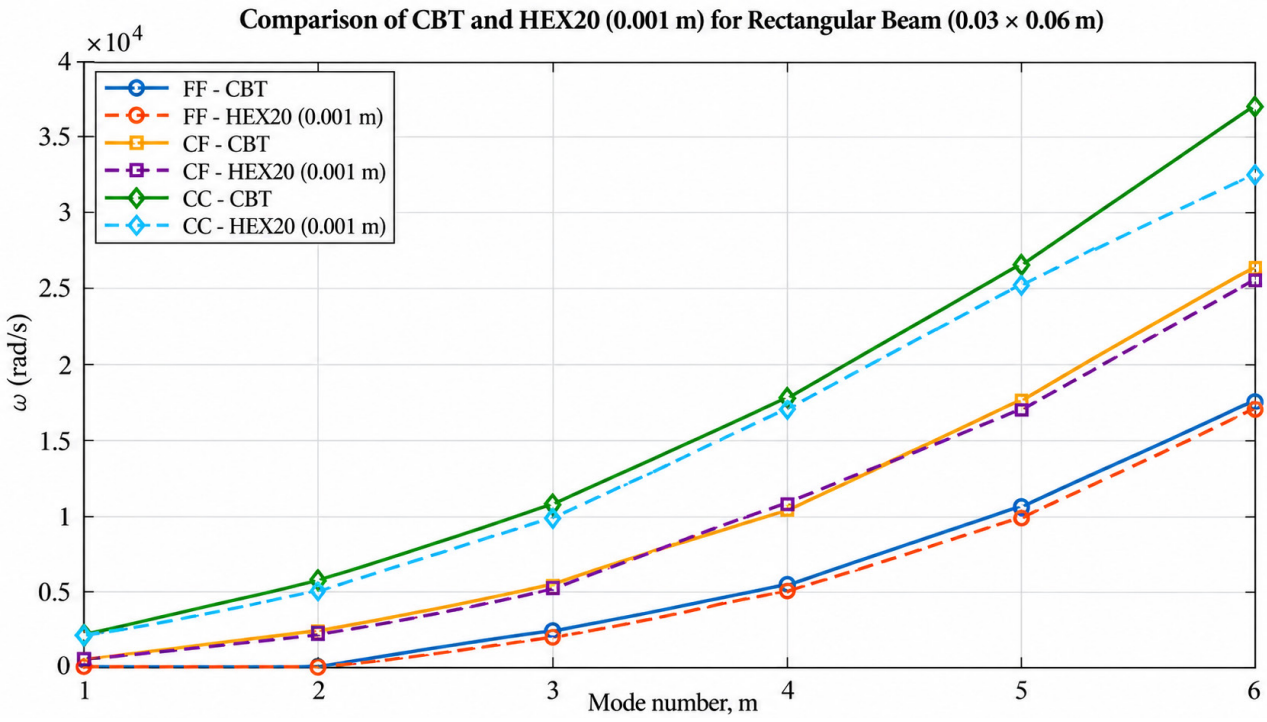


Figure 7. Comparison of CBT and ANSYS HEX20 results for rectangular beams (0.03×0.06 m)under FF, CF, and CC boundary conditions.

4.3.3. Mesh Convergence and Numerical Validation of Rectangular Beam Models

This section presents the modal results of rectangular beams obtained using Classical Beam Theory (CBT) and verified through MATLAB eigenvalue analysis. The analytical predictions are compared with 3D ANSYS simulations to evaluate numerical accuracy, mesh convergence behavior, and the reliability of the finite element discretization. Since rectangular cross sections do not possess a unique characteristic diameter, mesh refinement is characterized using the ratio h/b_{min} where b_{min} represents the minimum cross-sectional dimension governing bending curvature and stress gradients.

The novelty of this convergence assessment lies in using a geometry-based nondimensional mesh parameter, h/b_{min} instead of relying only on element size. This provides a more meaningful and transferable measure of mesh refinement for rectangular beam models. The convergence assessment is primarily based on Mode 3 because the lower modes converge rapidly and show limited sensitivity to mesh refinement, whereas Mode 3 exhibits stronger curvature effects and therefore provides a more rigorous evaluation of discretization quality. Higher modes are also monitored throughout the analysis to confirm the overall stability and consistency of the numerical formulation.

The ANSYS results show larger deviations for higher values of h/b_{min} particularly in the higher modes. As h/b_{min} decreases, the angular frequencies progressively stabilize and approach the analytical predictions. Further mesh refinement beyond this range produces only marginal changes, indicating mesh-independent numerical behavior. This provides strong evidence that the selected mesh density is sufficient to capture the bending-dominated modal response of rectangular beams. Therefore, the convergence study strengthens the credibility of the ANSYS model and supports its use for subsequent validation and parametric analysis. The corresponding convergence results for the third bending mode under CF boundary conditions are summarized in **Table 20**.

Table 20. Influence of normalized mesh size (h/b_{min}) on the third bending-mode frequency of rectangular beams under clamped–free boundary conditions.

Cross-section (m^2)	BC	Element size, h (mm)	h / b_{min}	Mode-3 f_n (Hz)
0.12 × 0.06	CF	0.01	0.167	10150.3
0.12 × 0.06	CF	0.005	0.083	10154.1
0.06 × 0.03	CF	0.005	0.167	5238.2
0.06 × 0.03	CF	0.001	0.033	5238.8

The results in **Figure 8** show stable third-mode frequency predictions as the mesh is refined, indicating consistent convergence behavior for the rectangular beam models. Since Mode 3 is more sensitive to discretization effects than the lower modes, its stable response provides a rigorous assessment of mesh quality, while the higher modes are also monitored to confirm the overall numerical stability of the formulation. The selected discretization therefore captures the dominant structural response with reliable accuracy without introducing unnecessary computational cost. Overall, the results support the robustness and applicability of the finite element formulation used for the rectangular beam analyses. The analytical and ANSYS results agree more closely for the lower and intermediate modes. At higher modes, the response becomes more sensitive to transverse shear deformation, beam rotary

inertia, and 3D stress effects. These effects are captured by the ANSYS solid model but are not included in the Euler–Bernoulli formulation.

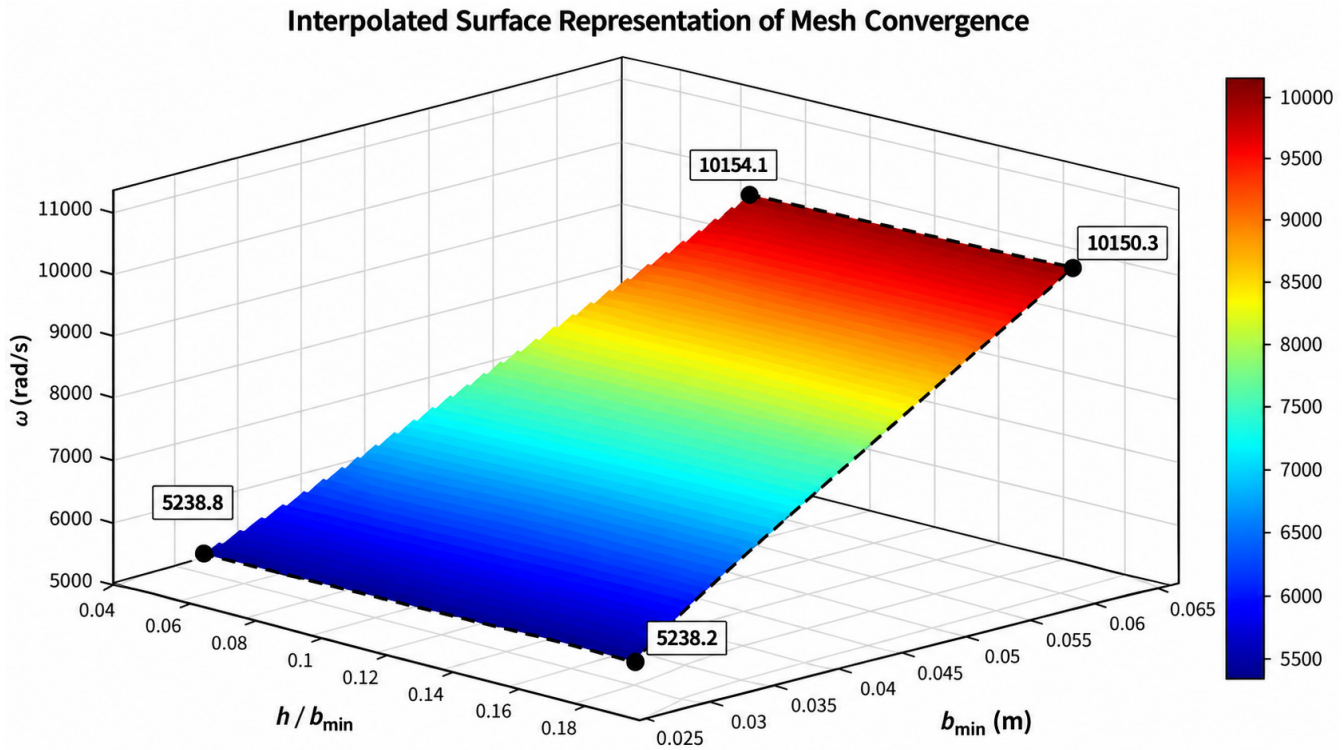


Figure 8. Interpolated surface plot illustrating the effect of normalized mesh size (h/b_{min})on the third bending-mode frequency of rectangular beams under clamped–free boundary conditions.

4.4. Effect of Intermediate Elastic Boundary Stiffness

To further demonstrate the applicability of the proposed formulation, the right-end translational and rotational spring stiffnesses were varied over several orders of magnitude. This represents elastic support conditions between the free and clamped limits. As the translational stiffness, (k_2), increased, the first natural frequency rose from 53.38 Hz to 226.53 Hz. The third natural frequency increased from 725.98 Hz to 1221.40 Hz. A similar trend was observed for rotational stiffness, (K_2).In this case, the first natural frequency increased from 152.29 Hz to 226.61 Hz, while the third natural frequency increased from 1022.40 Hz to 1224.10 Hz. The corresponding first-mode shapes were also examined to show the effect of boundary stiffness on the beam deformation. The results are presented in **Tables 21 and 22** and **Figure 9**. The remaining beam, mass, inertia, and left-end support parameters were kept constant.

Table 21. Effect of right-end translational stiffness, (k_2),on the first three natural frequencies (3D).

(k_2) (N/m)	(ω_1) (rad/s)	(ω_2) (rad/s)	(ω_3) (rad/s)	(f_1) (Hz)	(f_2) (Hz)	(f_3) (Hz)
21.476	335.41	1843.0	4561.5	53.382	293.32	725.98
2147.6	336.75	1843.2	4561.5	53.596	293.35	725.99
(2.1476×10^5)	449.27	1859.6	4567.3	71.504	295.97	726.91
(2.1476×10^7)	1359.7	3301.3	5427.6	216.41	525.42	863.83
(2.1476×10^9)	1423.3	3919.9	7674.3	226.53	623.87	1221.4

Table 22. Effect of right-end rotational stiffness, (K_2), on the first three natural frequencies (3D).

(K_2) (N•m/rad)	(ω_1) (rad/s)	(ω_2) (rad/s)	(ω_3) (rad/s)	(f_1) (Hz)	(f_2) (Hz)	(f_3) (Hz)
21.476	956.87	3093.1	6423.6	152.29	492.29	1022.4
2147.6	963.36	3099.4	6430.1	153.32	493.28	1023.4
(2.1476×10^5)	1232.5	3466.2	6878.2	196.16	551.66	1094.7
(2.1476×10^7)	1421.7	3915.0	7672.0	226.11	623.09	1221.0
(2.1476×10^9)	1423.8	3924.2	7691.2	226.61	624.56	1224.1

To As the right-end translational stiffness increases, the beam becomes more restrained, and the natural frequencies increase for all three modes. The same trend is observed for increasing rotational stiffness. At low stiffness values, the frequency changes are small. The effect becomes stronger as the support approaches the clamped condition. Higher modes are more sensitive because they involve greater curvature and rotation. These results show that both translational and rotational restraints strongly affect the beam vibration response. They also confirm that the proposed formulation can represent intermediate elastic support conditions accurately.

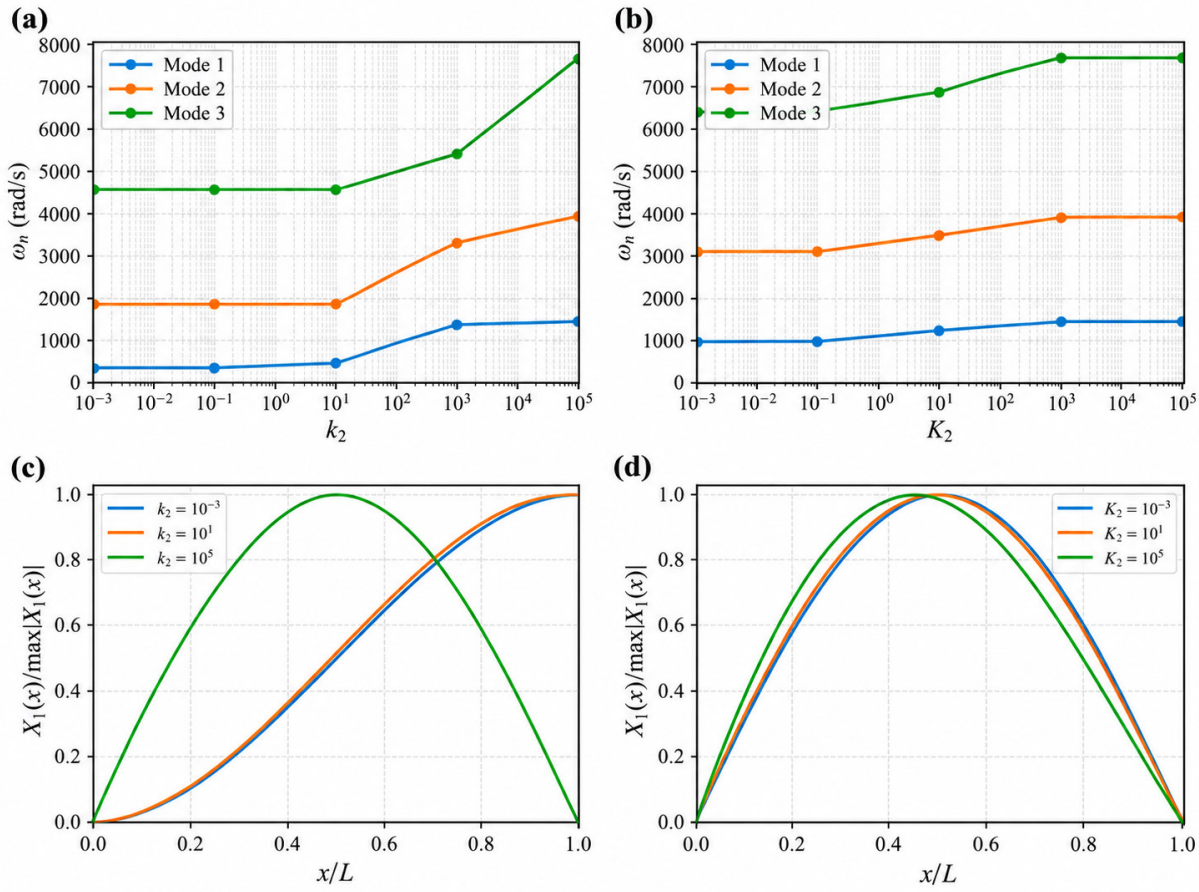


Figure 9. Effect of end-spring stiffness on beam vibration (a) natural frequencies versus translational stiffness, (k_2), (b) natural frequencies versus rotational stiffness, (K_2), (c) normalized first-mo shapes for selected (k_2) and (d) normalized first-mode shapes for selected (K_2).

4.5. Comparative Validation with Published Studies

To place the present results in context, selected literature findings are compared

with the analytical and numerical results of this study. The comparison focuses on beam vibration studies involving elastic supports, end attachments, and numerical validation. This helps clarify that the observed effects of stiffness, end mass, and mesh refinement are physically consistent with published results. It also supports the usefulness of the proposed compact analytical framework as a practical validation tool.

Table 22. Comparative summary of present results and selected literature on beams with elastic supports, attachments, and numerical validation

Reference	Configuration	Main observation	Quantitative result	Comparative relevance
Banerjee [14]	Cantilever beam with spring–mass system at the tip	Frequencies decrease with tip mass and increase with spring stiffness	Baseline non-dimensional frequencies: 3.5160, 22.034, 61.697, 120.90, 199.86	Confirms the same trend observed in the present study, where added mass lowers frequencies and added stiffness raises them
Pala and Kahya [13]	Elastically restrained cantilever Timoshenko beam with end attachment	Natural frequencies decrease with increasing end mass and increase with rotational spring stiffness	Parametric trends reported	Supports the present results on the influence of both boundary flexibility and end attachments
Kanwal et al. [11]	Elastically constrained beam on elastic foundation	Linear spring stiffness has a stronger influence than rotary stiffness	First four frequencies: 320.793, 658.137, 1122.622, 1612.209 Hz	Consistent with the present conclusion that stiffness parameters strongly affect modal response
Alkinidri et al. [20]	Beam spring system with varying stiffness	Consistent mass matrix gives much closer agreement with analytical values than lumped mass matrix	Relative errors as low as 1.01×10^{-7} (Mode 1) and 1.49×10^{-5} (Mode 2), for N = 50	Reinforces the importance of careful numerical modelling and convergence assessment in the present work
Present study	Circular beam, CF, (D = 0.10) m; CBT vs ANSYS HEX20 (0.005 m), Modes 1–6	Good agreement between analytical and 3D numerical results	Mean error = 5.72%; max error = 10.44%	Confirms the validity of the formulation for the clamped–free case
Present study	Circular beam, FF, (D = 0.05) m; CBT vs ANSYS HEX20 (0.001 m), Modes 3–6	Best agreement among the circular-beam cases	Mean error = 2.82%; max error = 5.45%	Shows strong agreement after mesh refinement
Present study	Circular beam, CF, (D = 0.05) m; CBT vs ANSYS HEX20 (0.001 m), Modes 1–6	Stable agreement between CBT and ANSYS results	Mean error = 3.51%; max error = 8.42%	Supports the reliability of the formulation for fixed–free beams
Present study	Circular beam, CC, (D = 0.05) m; CBT vs ANSYS HEX20 (0.001 m) Modes 1–6	Consistent agreement for the fixed–fixed case	Mean error = 3.52%; max error = 6.52%	Confirms robustness under higher restraint stiffness
Present study	Rectangular beam, CC, (0.03 m×0.06 m); CBT vs ANSYS HEX20 (0.001 m), Modes 1–6	Good overall agreement, with larger deviation in higher modes	Mean error = 6.13%; max error = 12.78%	Suggests a stronger influence of 3D effects in rectangular beams

The comparative analysis in **Table 22** shows that the main vibration trends reported in earlier studies are reproduced by the present formulation. Added mass reduces the natural frequencies, whereas higher boundary stiffness increases them. Similar behavior is observed for the FF, CF, and CC cases. **Table 22** also clarifies the contribution of the present study. The proposed formulation combines translational stiffness, rotational stiffness, end masses, and rotary inertia in one compact (4×4) characteristic matrix. This provides a direct way to analyze different boundary conditions within one framework.

The analytical and ANSYS results agree well for the lower and intermediate modes. The higher modes show larger differences because shear deformation, beam rotary inertia, and 3D effects become more important. These effects are captured by the ANSYS solid model but are not included in Euler–Bernoulli theory. The results therefore provide cross-verification of the proposed formulation.

5. Conclusion

This study developed a unified analytical framework for the free-vibration analysis of Euler–Bernoulli beams with elastic supports and lumped end masses. The formulation integrates translational stiffness, rotational stiffness, and discrete end inertia within a compact (4×4)characteristic matrix. The method allows efficient evaluation of natural frequencies and mode shapes under different boundary conditions.

The MATLAB results matched the classical reference solutions for the standard FF, CF, and CC cases. ANSYS HEX20 solid-element simulations were used for cross-verification and mesh-convergence assessment, rather than as absolute validation reference. Good agreement was obtained for the lower and intermediate bending modes of both circular and rectangular beams. Larger differences appeared in the higher modes, particularly for rectangular sections. These differences are associated with the different assumptions of the two models. The Euler Bernoulli model neglects transverse shear deformation, beam rotary inertia, warping, and other 3D effects that are included in the ANSYS solid model.

The results confirm that boundary flexibility and attached masses strongly influence modal characteristics and should be considered in realistic vibration analysis. The proposed formulation provides a simple and computationally efficient tool for preliminary modal analysis of beam-like structures with non-ideal support and attached components. It also provides an analytical benchmark for comparison with more advanced numerical models. The present work is limited to linear free vibration under small deformation. The supports and end masses are treated as idealized elements. Effects related to uncertain support stiffness, imperfect fixtures, damping, and assembly tolerances are not included. Experimental modal testing was also outside the scope of this study. Therefore, the results should be interpreted as analytical numerical cross-verification rather than complete experimental validation. The present model is most reliable for lower and intermediate bending modes within the applicability range of Euler–Bernoulli beam theory. For higher modes, relatively thick beams, uncertain support conditions, or applications requiring high-precision frequency prediction, a shear-deformable beam model and experimental modal testing should be considered. The deviations of up to approximately 10-13% in some higher-mode cases should be assessed according to the required design tolerance.

Limitations and Scope of the Present Model

The present model considers linear free vibration with small transverse deflection. It is intended mainly for slender beams, where bending is the dominant response. Transverse shear deformation and the rotary inertia of the beam itself are not included. Therefore, the results are more reliable for lower and intermediate modes. Accuracy may decrease for less slender beams and at higher frequencies.

The boundary springs and end masses are represented as idealized elements. In practice, support stiffness may vary, and fixtures can introduce damping, assembly tolerances, and local flexibility. These effects are not included in the present model. Experimental modal testing was also not part of this study. The results should therefore be viewed as analytical numerical cross verification, not complete experimental validation. For thick beams, high frequency vibration, or cases requiring close frequency prediction, a shear-deformable model and experimental testing should be used.

Author contributions: Conceptualization, Ahmed M. Zakwan and Mohammad S. Qatu; methodology, Ahmed M. Zakwan and Mohammad S. Qatu; software, Ahmed M. Zakwan; finite element modeling, Ahmed M. Zakwan; formal analysis, Ahmed M. Zakwan and Ibrahim M. Ashqar; writing-original draft preparation, Ahmed M. Zakwan; writing-review and editing, Ahmed M. Zakwan and Mohammad S. Qatu; supervision, Mohammad S. Qatu. All authors have read and agreed to the published version of the manuscript.

Funding: No funding was received for conducting this study or for preparing this manuscript.

Conflict of Interest: On behalf of all authors, the corresponding author states that there is no conflict of interest.

AI Use Statement: During the preparation of this manuscript, the authors used ChatGPT (OpenAI) for language editing and formatting support. No AI tools were used for data analysis, interpretation, or scientific content generation. The authors reviewed all content and took full responsibility for the final manuscript.

References

1. Augarde CE, Deeks AJ (2008) The use of Timoshenko's exact solution for a cantilever beam in adaptive analysis. Finite Elements in Analysis and Design 44:595–601. https://doi.org/10.1016/j.finel.2008.01.010
2. Avcar M (2014) Free Vibration Analysis of Beams Considering Different Geometric Characteristics and Boundary Conditions. mechanics 4:94–100. https://doi.org/10.5923/j.mechanics.20140403.03
3. Ruocco E, Reddy JN (2023) Analytical solutions of Reddy, Timoshenko and Bernoulli beam models: A comparative analysis. European Journal of Mechanics - A/Solids 99:104953. https://doi.org/10.1016/j.euromechsol.2023.104953
4. Mirzabeigy A, Madoliat R, Vahabi M (2017) Free vibration analysis of two parallel beams connected together through variable stiffness elastic layer with elastically restrained ends. Advances in Structural Engineering 20:275–287. https://doi.org/10.1177/1369433216649395
5. Vaz JDC, De Lima Junior JJ (2016) Vibration analysis of Euler-Bernoulli beams in multiple steps and different shapes of cross section. Journal of Vibration and Control 22:193–204. https://doi.org/10.1177/1077546314528366
6. Wang Y-R, Fang Z-W (2015) Vibrations in an elastic beam with nonlinear supports at both ends. J Appl Mech Tech Phy 56:337–346. https://doi.org/10.1134/S0021894415020200
7. Ike CC (2024) Critical buckling load analysis of Euler-Bernoulli beam on two-parameter foundations using Galerkin method. J mechatron, artif intell, eng 5:158–172. https://doi.org/10.21595/jmai.2024.24285
8. Cazzani A (2013) ON THE DYNAMICS OF A BEAM PARTIALLY SUPPORTED BY AN ELASTIC FOUNDATION: AN

EXACT SOLUTION-SET. Int J Str Stab Dyn 13:1350045. https://doi.org/10.1142/S0219455413500454
9. Motaghian SE, Mofid M, Alanjari P (2011) Exact solution to free vibration of beams partially supported by an elastic foundation. Scientia Iranica 18:861–866. https://doi.org/10.1016/j.scient.2011.07.013
10. Chen Y, Jin G, Liu Z (2013) Free vibration analysis of circular cylindrical shell with non-uniform elastic boundary constraints. International Journal of Mechanical Sciences 74:120–132. https://doi.org/10.1016/j.ijmecsci.2013.05.006
11. Kanwal G, Nawaz R, Ahmed N (2023) Analyzing the Effect of Rotary Inertia and Elastic Constraints on a Beam Supported by a Wrinkle Elastic Foundation: A Numerical Investigation. Buildings 13:1457. https://doi.org/10.3390/buildings13061457
12. Shi D, Wang Q, Shi X, Pang F (2015) An accurate solution method for the vibration analysis of Timoshenko beams with general elastic supports. Proceedings of the Institution of Mechanical Engineers, Part C: Journal of Mechanical Engineering Science 229:2327–2340. https://doi.org/10.1177/0954406214558675
13. Pala Y, Kahya C (2023) Free vibration analysis of elastically restrained cantilever Timoshenko beam with attachments. Pamukkale J Eng Sci 29:274–280. https://doi.org/10.5505/pajes.2022.93467
14. Banerjee JR (2012) Free vibration of beams carrying spring-mass systems − A dynamic stiffness approach. Computers & Structures 104–105:21–26. https://doi.org/10.1016/j.compstruc.2012.02.020
15. Xiao H, Sheng M, Liu Z, Wei Z (2013) The Study on Free Vibration of Elastically Restrained Beams Carrying Various Types of Attachments with Arbitrary Spatial Distributions. Shock and Vibration 20:369–383. https://doi.org/10.1155/2013/983451
16. Aydin E, Dutkiewicz M, Öztürk B, Sonmez M (2020) Optimization of elastic spring supports for cantilever beams. Struct Multidisc Optim 62:55–81. https://doi.org/10.1007/s00158-019-02469-3
17. Hang DT, Tung NX, Tu DV, Lam NN (2024) Finite Element Analysis of a Double Beam connected with Elastic Springs. Eng Technol Appl Sci Res 14:12482–12487. https://doi.org/10.48084/etasr.6489
18. Fei H, Zichen D, Danhui D (2022) A unified method for in-plane vibration analysis of double-beam systems with translational springs. Journal of Sound and Vibration 534:117042. https://doi.org/10.1016/j.jsv.2022.117042
19. Osuji SO, Adegbemileke SA (2015) Modelling Convergence of Finite Element Analysis of Cantilever Beam. 30:
20. Alkinidri M, Nawaz R, Alahmadi H (2024) Analytical and numerical investigation of beam-spring systems with varying stiffness: a comparison of consistent and lumped mass matrices considerations. MATH 9:20887–20904. https://doi.org/10.3934/math.20241016
21. Chen D, Gu C, Li M, et al (2022) Natural vibration characteristics determination of elastic beam with attachments based on a transfer matrix method. Journal of Vibration and Control 28:637–651. https://doi.org/10.1177/1077546320980643
22. Gasbarri P, Monti R, Sabatini M (2014) Very large space structures: Non-linear control and robustness to structural uncertainties. Acta Astronautica 93:252–265. https://doi.org/10.1016/j.actaastro.2013.07.022
23. Zakwan AM, Qatu MS (2026) A Multi Fidelity Framework Integrating CLT, Vinson–Sierakowski Method, and 3D Finite Element Analysis for Modal Prediction and Parametric Design of Symmetrically Laminated CFRP Beams. Journal of Composites Science 10:421. https://doi.org/10.3390/jcs10080421
24. Qin B, Zhao X, Liu H, et al (2020) Free Vibration Analysis of Curved Laminated Composite Beams with Different Shapes, Lamination Schemes, and Boundary Conditions. Materials 13:1010. https://doi.org/10.3390/ma13041010
25. Shi Z, Yao X, Pang F, Wang Q (2017) An exact solution for the free-vibration analysis of functionally graded carbon-nanotube-reinforced composite beams with arbitrary boundary conditions. Sci Rep 7:12909. https://doi.org/10.1038/s41598-017-12596-w
26. Xu J, Yang Z, Yang J, Li Y (2021) Influence of the boundary relaxation on the free vibration of rotating composite laminated Timoshenko beams. Composite Structures 266:113690. https://doi.org/10.1016/j.compstruct.2021.113690
27. Jin Y, Lu Y, Yang D, et al (2024) An analytical method for vibration analysis of multi-span Timoshenko beams under arbitrary boundary conditions. Arch Appl Mech 94:529–553. https://doi.org/10.1007/s00419-023-02534-w
28. Wang P, Wu N, Luo H, Sun Z (2021) STUDY ON VIBRATION RESPONSE OF A NON-UNIFORM BEAM WITH NONLINEAR BOUNDARY CONDITION. FU Mech Eng 19:781. https://doi.org/10.22190/FUME210324045W
29. Zhang Z, Zhao Y, Mi X, et al (2025) Vibration reduction study of an elastic beam by utilizing an extension beam and a boundary nonlinear connector. Nonlinear Dyn 113:14607–14627. https://doi.org/10.1007/s11071-025-10920-y
30. Bert CW, Malik M (1997) Differential quadrature: A powerful new technique for analysis of composite structures. Composite Structures 39:179–189. https://doi.org/10.1016/S0263-8223(97)00112-8
31. Kabir H, Aghdam MM (2021) A generalized 2D Bézier-based solution for stress analysis of notched epoxy resin plates

reinforced with graphene nanoplatelets. Thin-Walled Structures 169:108484. https://doi.org/10.1016/j.tws.2021.108484

32. Maiz S, Bambill DV, Rossit CA, Laura PAA (2007) Transverse vibration of Bernoulli–Euler beams carrying point masses and taking into account their rotatory inertia: Exact solution. Journal of Sound and Vibration 303:895–908. https://doi.org/10.1016/j.jsv.2006.12.028
33. Leissa AW, Qatu MS (2011) Vibrations of Continuous Systems. The McGraw-Hill Companies